Journal of proteome research

Article

pubs.acs.org/jpr

Liver Metabolomics Reveals Increased Oxidative Stress and Fibrogenic Potential in Gfrp Transgenic Mice in Response to Ionizing Radiation

Amrita K Cheema,*[,†,‡,●] Rupak Pathak,[§,●] Fereshteh Zandkarimi,[†] Prabhjit Kaur,[†] Lynn Alkhalil,[†] Rajbir Singh,[†] Xiaogang Zhong,[∥] Sanchita Ghosh,[⊥] Nukhet Aykin-Burns,[§,●] and Martin Hauer-Jensen[§,●]

[†]Departments of Oncology, [‡]Biochemistry, Molecular and Cellular Biology, and [∥]Department of Biostatistics, Bioinformatics and Biomathematics, Georgetown University Medical Center, Washington DC 20057, United States

[§]Division of Radiation Health, College of Pharmacy, University of Arkansas for Medical Sciences, Little Rock, Arkansas, Central Arkansas Veterans Healthcare System, Little Rock, Arkansas 72205, United States

[⊥]Armed Forces Radiobiology Research Institute, Uniformed Services University of the Health Sciences (USUHS), Bethesda, Maryland 20889-5603, United States

Supporting Information

ABSTRACT: Although radiation-induced tissue-specific injury is well documented, the underlying molecular changes resulting in organ dysfunction and the consequences thereof on overall metabolism and physiology have not been elucidated. We previously reported the generation and characterization of a transgenic mouse strain that ubiquitously overexpresses Gfrp (GTPH-1 feedback regulatory protein) and exhibits higher oxidative stress, which is a possible result of decreased tetrahydrobiopterin (BH4) bioavailability. In this study, we report genotype-dependent changes in the metabolic profiles of liver tissue after exposure to nonlethal doses of ionizing radiation. Using a combination of untargeted and targeted quantitative mass spectrometry, we report significant accumulation of metabolites associated with oxidative stress, as well as the dysregulation of lipid metabolism in transgenic mice after radiation exposure. The radiation stress seems to exacerbate lipid peroxidation and also results in higher expression of genes that facilitate liver fibrosis, in a manner that is dependent on the genetic background and post-irradiation time interval. These findings suggest the significance of Gfrp in regulating redox homeostasis in response to stress induced by ionizing radiation affecting overall physiology.

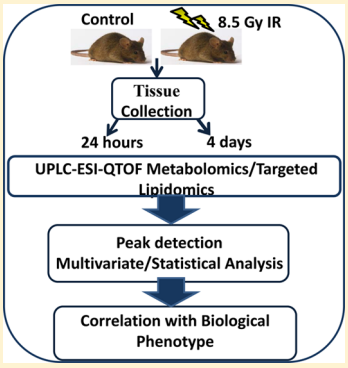

KEYWORDS: *metabolomics, ionizing radiation, stress signaling*

INTRODUCTION

The liver is a vital organ primarily responsible for detoxification, emulsification of fats, and maintenance of constant blood glucose levels.[1] The molecular mechanism of liver injury as a consequence of ionizing radiation (IR) exposure, especially in the context of concomitant radiotherapy, is not well understood.[2−5] IR can cause perturbations in RNA and protein expression patterns, which may lead to enhanced oxidative stress and subsequent cell death. There is, however, a paucity of studies that evaluate direct effects of radiation-induced liver tissue injury and its implications on organ function and metabolism. Recently, metabolomic studies based on nuclear magnetic resonance spectroscopy (NMR) and gas chromatography−mass spectrometry (GC-MS) have reported several metabolic biomarkers of radiation exposure in biofluids such as urine and blood plasma using animal models.[6−8] Metabolomic read out of cellular processes is increasingly gaining credence as an approach to identify biomarkers of IR exposure and to understand the metabolic changes accompanying radiation exposure.[9−12]

Tetrahydrobiopterin (BH4) is a natural antioxidant and its de novo synthesis is strictly regulated by the enzyme GTP cyclohydrolase-1 (GTPCH-1).[13] The enzymatic activity of GTPCH-1 can be inhibited by GTPCH-1 feedback regulatory protein (Gfrp), resulting in low BH4 bioavailability and increased oxidative stress.[14] We have recently developed a novel, overexpressed Gfrp "knock-in" transgenic mouse that shows decreased levels of total glutathione (GSH) and a higher percentage of glutathione disulfide (GSSG) in peripheral blood compared to its control littermates at the basal level.[15] Therefore, this mouse model could be used as an in vivo model of elevated oxidative stress. Moreover, this mouse model may provide valuable insights toward understanding the role of BH4-mediated redox homeostasis in normal tissue injury in response to IR.

Radiation is known to generate reactive oxygen species (ROS) resulting in oxidative stress.[16] In order to detoxify the

Received: March 17, 2014
Published: May 13, 2014

detrimental effects of excess ROS, the liver has an array of antioxidant systems that include enzymatic and nonenzymatic components. BH4 is one of the key nonenzymatic components of the antioxidant system and is known to be down-regulated by IR.[17] BH4 also regulates the catalytic activity of enzymes involved in maintaining cellular redox balance, including endothelial nitric oxide synthase (eNOS). Therefore, impairment of BH4 biosysnthesis and/or exposure to IR may likely disrupt redox homeostasis, which in turn may modulate molecular targets of fibrosis which is generally considered as a delayed effect of IR exposure.

We set out to determine the role of Gfrp overexpression on liver metabolic profiles, particularly with respect to oxidative stress and fibrosis, in irradiated mice. Gfrp transgenic mice and their control littermates were exposed to a nonlethal dose of 8.5 Gy of total body irradiation (TBI). Liver tissue was collected at 24 h and 4 days postirradiation to investigate acute and subacute radiation effects, respectively, on biochemical and metabolic responses. The radiation dose and the postirradiation time of tissue collection in this study were selected because of following reasons: (a) current study was undertaken as a further extension of our previous findings, (b) to find out the role of liver metabolites, especially involved in oxidative stress and fibrosis, in making Gfrp transgenic mice more susceptible to IR under identical experimental conditions as observed in our previously published results, (c) no mortality of mice is expected within the time frame and radiation dose used in this study as confirmed from previously published survival data, and (d) previous reports show that a dose of 6 Gy or more of TBI is required to induce change in liver fibrogenic profile.[18,19] We used ultraperformance liquid chromatography (UPLC) coupled with electrospray ionization mass spectrometry (ESI-MS) to perform untargeted small molecule metabolite profiling of matched sham and irradiated groups. Subsequently, stable isotope dilution multiple reaction monitoring mass spectrometry was used to confirm distinct changes in lipid and amino acid metabolism based on treatment and genetic background of mice. We observed that radiation exposure causes enhanced lipid peroxidation and increased expression of genes known to promote liver fibrosis in Gfrp knock-in mice as compared to their control littermates. Taken together, our data demonstrate that Gfrp overexpressing mice exhibit higher susceptibility to a compromised liver function in response to radiation exposure.

MATERIALS AND METHODS

Reagents and Standards

Acetonitrile (ACN), methanol, and water (LC-MS grade) were purchased from Fisher Scientific (NJ, U.S.A.). Debrisoquine, 4-nitrobenzoic acid (4-NBA) was purchased from Sigma (U.S.A.). All compounds used for validation of metabolite identification were bought from Sigma, and the lipid standards were purchased from Avanti Polar Lipids, Inc. (Alabama, U.S.A.).

Transgenic Mice Generation, Transgene Expression, and Animal Maintenance

The details of Gfrp transgenic mice generation and the mechanism of transgene overexpression have been described elsewhere.[15] Briefly, the plasmid construct containing Gfrp transgene was introduced in the C57BL/6 embryos by microinjection to develop the Gfrp founders, and the transgene was subsequently allowed to express in F1 generation mice by crossing Gfrp male founders with *EIIaCre* female mice (stock no. 003724; The Jackson Laboratory, CA, U.S.A.), which allows ubiquitous Gfrp transgene overexpression in F1 generation mice that bear a single copy of the transgene, whereas the littermates lacking the transgene were used as wild-type control mice. The presence of transgene in F1 generation mice was detected by tail DNA genotyping using transgene specific PCR primers.[15] Ten to 12 weeks old F1 generation male mice with an average body weight of 23 to 26 g were used in this study. All mice were kept in a temperature-controlled room with a 12 h light/dark cycle and provided with regular chow (Harlan Teklad laboratory diet 7012, Purina Mills, St. Louis, MO) and water. All animal procedures were performed in accordance with a protocol approved by the Central Arkansas Veterans Healthcare System Institutional Animal Care and Use Committee. Research was conducted according to the Guide for the Care and Use of Laboratory Animals, prepared by the Institute of Laboratory Animal Resources, the National Research Council, and U.S. National Academy of Sciences.

Radiation Exposure

Irradiation was performed with a J. L. Shepherd Mark I, model 25 ^{137}Cs irradiator (J. L. Shepherd & Associates, San Fernando, CA). Unanesthetized mice were placed in cylindrical, well-ventilated Plexiglas chambers (J. L. Shepherd & Associates) divided into four 90° "pie slice" compartments by vertical dividers made of T-6061 aluminum (machinable grade) with a gold anodized coating. Two chambers were stacked on top of each other and placed on a turntable rotating at 5 rpm in the position furthest away from the radiation source, allowing eight mice to be irradiated at a time. The average dose rate was 1.21 Gy per minute, and mice were exposed to 8.5 Gy of total body irradiation. Dose uniformity was assessed by thermoluminescence dosimetry (TLD). Tissue-equivalent mouse phantoms were placed into each of the compartments of the same Plexiglas chambers used for irradiation. Two Harshaw TLD-100 lithium fluoride chips were placed into the center of each phantom and exposed to radiation with the turntable rotating. The irradiated TLD chips and unirradiated control chips were subsequently analyzed by an independent company (K&S Associates, Inc., Nashville, TN). Groups of four to eight mice were euthanized humanely at set postirradiation time intervals (24 h and 4 day). Mice abdominal cavity was opened with a fine scissor and liver tissue was collected in a 1.5 mL Eppendorf tube. The collected tissue was immediately snap frozen in liquid nitrogen and finally stored in −80 °C until further use. Samples from individual mouse were analyzed separately throughout the experiment, without pooling the samples from different animals of the same group. For all assays, four to six mice per genotype per treatment group were included.

Metabolite Extraction

Sample preparation for metabolite extraction was performed as described previously.[20] Briefly, 200 μL of 50% chilled methanol (MeOH/H2O, 1:1 v/v) containing internal standards was added to tissue sections in MagNA Lyser tubes containing ceramic beads. The samples were homogenized using three 30 s pulses in a MagNA Lyser homogenizer (Roche, U.S.A.) at 7000 rpm. The supernatant was transferred to a fresh tube, and 400 μL of chilled 100% ACN was added. The pellets were used for protein quantification using the Bradford method. The samples were incubated on ice for 15 min and centrifuged at 13 000 rpm at 4°C for 15 min. The supernatant was transferred to a fresh tube and dried under vacuum. The samples were resuspended in 300 μL of solvent containing 95% water, 5% MeOH for mass spectrometry analysis.

UPLC-ESI-Q-TOF-MS Profiling

Metabolites extracted from control and irradiated tissue samples were analyzed as a single injection for each sample. Five microliters of each sample was injected onto a 50 mm × 2.1 mm Acquity 1.7 μm C18 column using an Acquity UPLC system online with electrospray quadrupole-time-of-flight tandem mass spectrometer (ESI-Q-TOF) (QTOF Premiere, Waters Corp, Milford, MA). The gradient mobile phase consisted of 0.1% formic acid (A) and acetonitrile containing 0.1% formic acid (B). The instrument was operated with a capillary voltage of 3.2 kV and a sampling cone voltage of 35.0 V in positive mode with a flow rate of 0.5 mL/min. The other conditions comprise the following: extraction cone voltage, 2.7 V; source temperature, 120 °C; desolvation temperature, 350 °C; desolvation gas flow rate, 800 L/h; cone gas flow rate, 25 L/h. Mass spectra were acquired over the mass range of 50−1200 m/z in the centroid mode. A 500 pg/μL solution of sulfadimethoxine in 50% acetonitrile ($[M + H]^+$, m/z 311.0814) was infused at 0.08 μL/min flow rate as the reference mass (lock mass) for accurate mass measurements. The quality control samples comprised an aliquot of all samples (all groups and time points) in the study set, thus representing a universal set of metabolites for this study. Initially, the column was conditioned using this QC sample, and thereafter it was injected after every 10 injections to account for reproducibility of the LC-MS data. The coefficient of variance for the QC samples was less than 5%. This approach has been recommended as a standard practice leading metabolomics researchers.[21]

LC-MS Data Processing

The UPLC-QTOF raw data files were converted into NetCDF format (Network Common Data Form) using the MassLynx software (Waters Corp, Milford, MA). Subsequently, the LC-MS data were preprocessed using XCMS software, as has been described previously.[22] For untargeted metabolomic profiling detailed in this study, the internal standards were added before extraction by spiking the extraction buffer with a known concentration of internal standards to account for variability in the extraction procedure as well as during MS-based data acquisition. Subsequently, the data were normalized to the internal standards and to the total protein concentration. The data were log transformed before further analysis. Relative quantitation was achieved for molecular ions using the UPLC-QTOF system by taking a ratio of normalized intensity of the respective sham and irradiated groups for the ions of interest. This approach has been used by several laboratories including ours in previously reported studies.[10,23−25] In order to ensure data quality and reliability, a test mix of standard metabolites was injected at the beginning and at the end of the batch and the extracted ion chromatograms were evaluated for mass accuracy and sensitivity with respect to intensity for the given standards. The normalized data were processed using MetaboAnalyst software (2.0)[26] using univariate and multivariate analysis methods. PLS-DA was used for checking the assumption that the groups of interest are different from each other and to assess the "goodness" of the model using R^2 and Q^2 as descriptors of model quality. We employed a 10-fold cross-validation method in Metaboanalyst to determine the optimal number of components to the model. The candidate markers were selected by examining the volcano plot by considering fold-change threshold of 2 and statistical p-value less than 0.05. These metabolites were initially identified based on their m/z against Metabosearch, which inquires accurate mass-based identification through four main online databases: the Human Metabolome Database (HMDB), Lipid Maps, Madison Metabolomics Consortium Database (MMCD), and Metlin.[27] The identity of metabolites was then confirmed by comparisons of fragmentation spectra and retention time with pure standards using tandem mass spectrometry (MS/MS). Signal intensities of the differentially abundant metabolites were visualized as a heat map. As mentioned previously, the raw data were log transformed and hierarchically clustered by Pearson correlation and average linkage clustering.

Lipid Peroxidation Assay

The mouse tissues were sonicated in RIPA buffer with protease inhibitor for 3 cycles of 15 s each on ice. The tubes were centrifuged at 14 000 rpm for 10 min at 4 °C. The supernatant was used for the lipid peroxidation assay. The assay was performed using the TBARS kit (Cayman Chemicals, U.S.A.) as per the manufacturer's instructions. Briefly, samples or standard MDA was mixed with 4 mL of assay reagent (containing TBA acetic acid and TBA sodium hydroxide). The vials were tightly capped and kept in a boiling water bath for 1 h and subsequently transferred to ice for 10 min to quench the reaction. The vials were centrifuged at 14 000 rpm for 10 min at 4 °C. From each vial, 150 μL of the supernatant was transferred to a clear 96-well plate, and the absorbance was read at 530 nm and corrected using a blank. The corrected absorbance of MDA was plotted as a function of MDA concentration, and the concentration of MDA for each sample was extrapolated from the standard curve. MDA (μM) = [corrected absorbance − y intercept/slope]. ANOVA (analysis of variance) was performed to test the significance of change in different biological groups at different time points.

Mouse Fibrosis Array

Isolation of RNA. The liver tissues were stabilized in RNALater before isolation. The RNA was isolated using RNA extraction kit (RNAeasy, Qiagen). Briefly, the tissues were homogenized using Powergen-125 homogenizer in 250 μL of RLT buffer. The lysate was centrifuged at 14 000 rpm for 2 min. Supernatant was carefully removed and transferred to an eppendorf tube followed by addition of 1 vol of 70% ethanol and mixed by pipetting. The lysate was loaded to the spin column placed in a 2 mL collection tube and centrifuged at 14 000 rpm for 30 s to collect RNA in RNase-free water.

cDNA Synthesis. The cDNA was synthesized using first strand synthesis kit (SA Biosciences). The reagents of the kit were thawed on ice and spun briefly. Genomic DNA elimination mix was made as 1000 ng of RNA, 2 μL of buffer and RNase-free water to make the total volume of 10 μL. The mix was incubated at 42 °C for 5 min and immediately placed on ice for at least 1 min. Reverse-transcriptase mixture was added to tube containing 10 μL of DNA elimination mix, the mixture was mixed well and incubated at 42 °C for 15 min, and the reaction was stopped by immediately incubating at 95 °C for 5 min. The reaction was quenched by the addition of RNase-free water.

Real-Time PCR for RT^2 Profiler PCR Array. The RT^2 Profiler PCR array (Mouse fibrosis array kit, QIAGEN, U.S.A.) was purchased from Qiagen as a 96-well kit. Each well is coated with one gene-specific primer (84 genes) along with five housekeeping genes, one genomic DNA contamination (MGDC), and three positive PCR controls. A master mix containing a defined volume and concentration ratio of RT^2

dx.doi.org/10.1021/pr500278t | J. Proteome Res. 2014, 13, 3065−3074

SYBR Green, cDNA synthesis reaction mixture, and RNase free water was prepared, and 25 μL of this mix was added to each well of the PCR array with the help of multichannel pipet. Q-PCR was performed on ABI PRISM 7900HT Sequence Detection System (Applied Biosystems, Foster City, CA). Cycle threshold values for each reaction were adjusted automatically. The fold-change values were derived relative to the control and normalized with the house keeping genes. The reaction cycle was set as Stage 1−95 °C for 10 min, Stage 2−95 °C for 15 s, followed by 60 °C for 1 min with repeats (40 cycles) and with the dissociation stage. The experiment was run in standard mode. Data analysis was performed using Graphpad prism software.

Stable Isotope Dilution − Multiple Reaction Monitoring Mass Spectrometry (SID-MRM-MS)

Targeted metabolomic analysis of liver tissue samples was performed using the Biocrates Absolute-IDQ P180 (BIOCRATES, Life Science AG, Innsbruck, Austria). This targeted assay allows for simultaneous detection and quantification of metabolites in biological matrices in a high-throughput manner.[28,29] Metabolite extraction from the tissue samples was performed by homogenizing in 50% methanol and subsequently processed as per the instructions by the manufacturer and analyzed on a triple quadrupole mass spectrometer (Xevo TQ-S, Waters Corporation, U.S.A.) operating in the MRM mode. The measurements were made in a 96-well format for a total of 34 tissue samples from Gfrp (WT and transgenic) mice that were sham irradiated or collected after 24 h and 4 days of radiation exposure, seven calibration standards, and three quality control samples that were integrated in the kit. Briefly, the flow injection analysis (FIA) tandem mass spectrometry (MS/MS) method was used to quantify a panel of 144 lipids including 39 acylcarnitines, 15 sphingomyelins, and 90 phosphatidylcholines simultaneously by multiple reaction monitoring. The targeted analysis of lipids using flow injection analysis has been tested for linearity over a broad concentration range using lipid standards. The other metabolites including amino acids and biogenic amines were resolved on the UPLC and quantified using scheduled MRMs. Data were normalized to the total protein concentration of tissue lysates and analyzed using the MetIQ software (Biocrates, Inc.). The samples were run as triplicates, and the coefficient of variance of individual metabolites was ≤15%. Quality control samples were used to assess reproducibility of the assay, which includes lipids of all classes. Difference detection was performed using the Metaboanalyst statistical tool suite.[30]

RESULTS

Identification of Markers of Radiation Exposure in Liver Tissue Extracts in Control Gfrp Mice

We performed comparative metabolomic profiling of liver tissue obtained from sham-treated mice or those exposed to 8.5 Gy of IR, in sham and IR treated groups, after 24 h or 4 days of radiation exposure. Preprocessing using XCMS resulted in a three-dimensional data matrix (m/z, retention time, and intensity values) consisting of a total of 1477 (24 h) and 1473 (4 days) features that were subsequently used for multivariate analyses (Table 1). Consequently, a partial least square−discriminant analysis (PLS-DA) was performed to delineate putative metabolites that contribute to class separation. At 24 h and at 4 days, the R^2 and Q^2 values were

Table 1. Statistically Significant Features in Mouse Liver Tissue after 8.5 Gy Radiation Doses at 24 h and 4 Day Time Points

genotype	time	no. of features
total no. of features post XCMS processing		
Gfrp−/Cre+	24 h	1477
	4 days	1473
Gfrp Tg, Gfrp+/Cre+	24 h	1481
	4 days	1482
total no. of significantly deregulated features for different genotypes		
Gfrp−/Cre+	24 h	50
	4 days	71
Gfrp Tg, Gfrp+/Cre+	24 h	53
	4 days	176

[a]Top 50 metabolites of each set (lowest p-values, $p < 0.05$ and with a fold change greater than two) were putatively identified using a mass-based database search and later confirmed using tandem mass spectrometry.

0.93 and 0.76 and 0.99 and 0.72, respectively, yielding good support for the model quality (Figure 1A,C). Finally, the candidate markers were selected by examining the volcano plot and considering a fold-change threshold of 2 and p-value less than 0.05 (Figure 1B,D). The features contributing to the segregation from both analyses were chosen for accurate mass-based identification. Identities of some of these metabolites were confirmed by tandem mass spectrometry (Supplementary Table 1, Supplementary Figures S1−S3). The control mice showed a significant decrease in the levels of metabolites like bilirubin, cytidine, and adenosine monophosphate after radiation exposure. It has been reported that bilirubin can protect lipid from peroxidation.[31] Therefore, a decrease in the levels of bilirubin can increase the risk of formation of free radicals and increase lipid peroxidation in the liver.[32−34] The levels of secondary bile acids such as sulfoglycolithocholate increased significantly (Supplementary Table 2) after 24 h of radiation exposure. We also found dysregulation of several lipid metabolites including sphingomyelins, phosphatidyl glycerol (PG), phosphatidyl ethanolamine (PE), phosphatidyl serine (PS), and ceramides in irradiated mice, after 4 days of radiation exposure. Such metabolic perturbations emphasize the central role of liver in regulating lipid metabolism.[35]

Increased Oxidative Stress Metabolites in Gfrp Knock-In Mice after Radiation Exposure

Metabolomic profiling of transgenic mice was performed under the same conditions to delineate genotype-dependent markers of radiation-induced tissue injury in liver. We have previously reported that this mouse model exhibits higher basal oxidative stress than the wild-type littermates.[18] LC-MS data preprocessing using XCMS resulted in approximately 1480 features. Multivariate analysis showed significant dysregulation of 53 features after 24 h and 176 markers after 4 days of radiation exposure (Table 1). Difference detection analysis revealed intrinsic changes in metabolic profiles after 24 h and 4 days of radiation exposure (Figure 2). Some of these metabolites were unambiguously identified by matching retention time and fragmentation pattern (Supplementary Table 3 and Supplementary Figures S4−S14) with standards while others were identified by matching fragmentation pattern of the compounds against a spectral library (Supplementary Figures S15−S16). Similar to the response of wild-type mice to irradiation, we found dysregulation of a broad class of lipids as well as sugars in

dx.doi.org/10.1021/pr500278t | J. Proteome Res. 2014, 13, 3065−3074

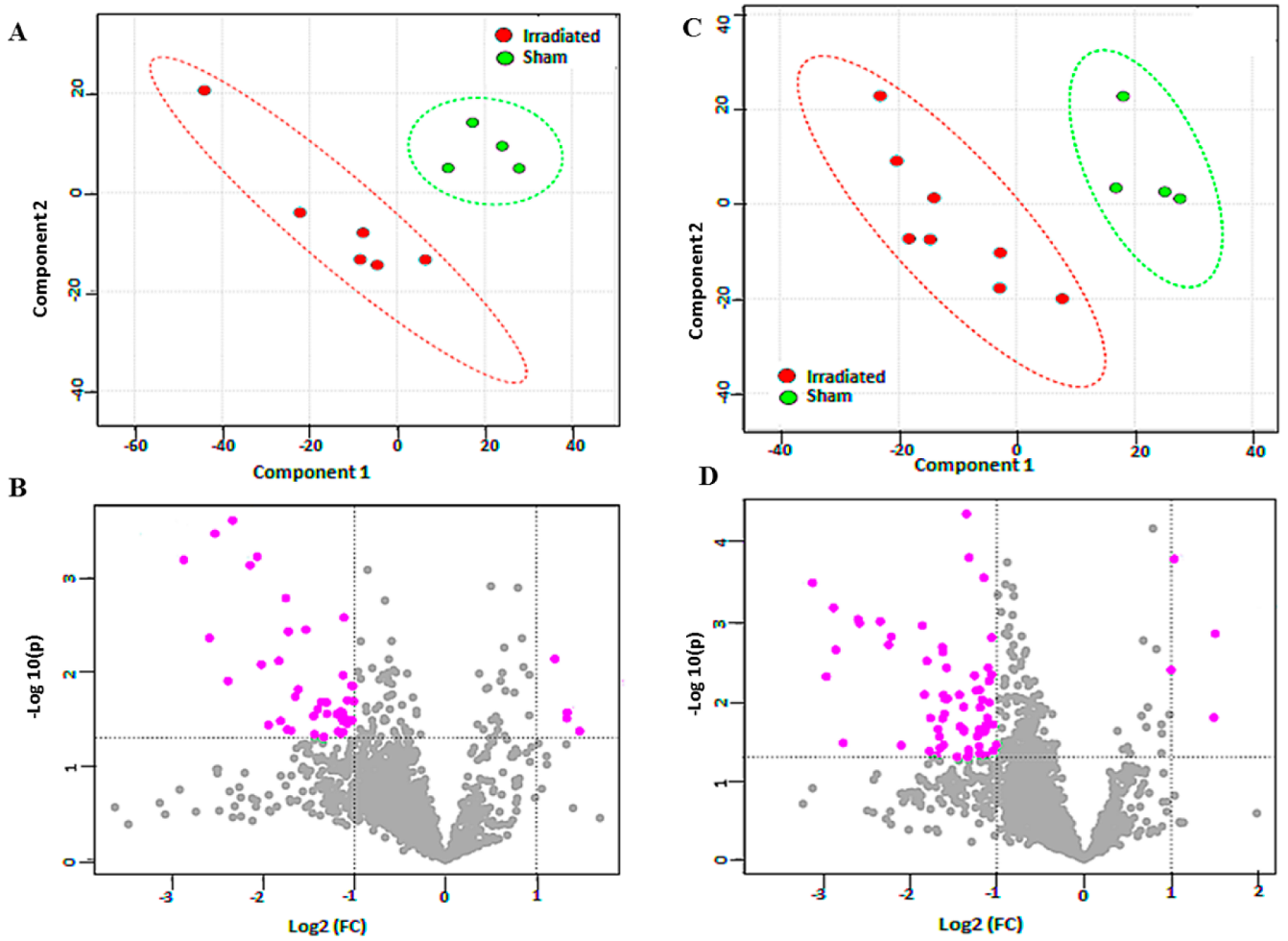

Figure 1. Comparative metabolomic profiling in Gfrp−/Cre+ (control) mice. (A,C) PLS-DA score plots of mice tissue samples analyzed in the positive electrospray ionization mode comparing liver metabolite profiles from mice that were euthanized 24 h or 4 days postradiation exposure, respectively, to those that were sham irradiated. (B,D) Volcano plot of liver metabolic profiles in the same order. Volcano plot indicates the size of the biological effect (fold change) versus the statistical significance of the result (statistical *p*-value). Each dot represents a metabolite plotted as a function of fold change (log 2 (fold change), *x*-axis) and statistical significance (−log 10 (*p*-value), *y*-axis). The pink dots represent selected putative markers with a *p*-value ≤0.05 and fold-change cutoff of > or < 2.

irradiated transgenic mice after 24 h and 4 days. Furthermore, we observed a significant increase in the level of bile acids including cholic acid and its derivatives such as taurocholic acid and taurodeoxycholic acid after 4 days and decreased levels of lipids such as of PC and PI lipids after 24 h after irradiation (Figure 3). These results may support previous reports[34,36] that bile acid accumulation in the liver can enhance generation of ROS and the formation of lipid peroxidation caused by radiation-induced liver injury, and this increase is more pronounced in transgenic mice. An increase in the levels of 12(13) - EpOME (epoxide of linoleic acid) after 4 days of radiation exposure may be indicative of increased inflammatory gene expression and increased oxidative stress leading to neutrophil accumulation in the liver.[37] We also observed a significant increase in arachidonic acid levels (C20:4), which is known to be an inflammatory mediator by activation of phospholipases,[38,39] wherein the phospholipases hydrolyze the sn-1 (PLA_1) or sn-2 (PLA_2) acyl bond of phospholipids. For example, the fold change (irradiated/sham) after 4 days exposure to radiation of Lyso-PC (20:4) /PC (20:4/14:0) and Lyso-PC (20:4)/ PC (18:1/20:4), were calculated to be 2.30 and 2.25, respectively. These results suggest that exposure to radiation may increase inflammation response in liver of transgenic mice. In addition, glycerophospho-inositol (PI) levels were decreased significantly after 4 days exposure to radiation. PIs have an important role as signaling molecules as mediators of immune responses in the body.[40] The depletion of PIs may exacerbate the inflammatory response and cause liver damage and compromised immune response.

Although our initial aim was to understand the genotype-dependent response to radiation exposure, we asked whether these metabolites show a common trend in both genotypes over time. For this purpose, the differentially abundant metabolites from independent analyses (Figures 1 and 2) were visualized as a heat map (Figure 3). Interestingly, GSSG levels were significantly increased 4 days following IR in the livers of wild-type mice. This increase in GSSG levels was also accompanied by increased levels of total GSH, keeping the GSSG of the irradiated wild-type mice at the same levels of sham-irradiated wild-type animals. This result suggests that wild-type mice responded to IR-induced oxidative stress by up-regulating the levels of hepatic glutathione; thus maintaining similar levels of GSSG observed in the control (sham-irradiated group). Percentage of GSSG levels were not affected at the 24 h

dx.doi.org/10.1021/pr500278t | *J. Proteome Res.* 2014, 13, 3065−3074

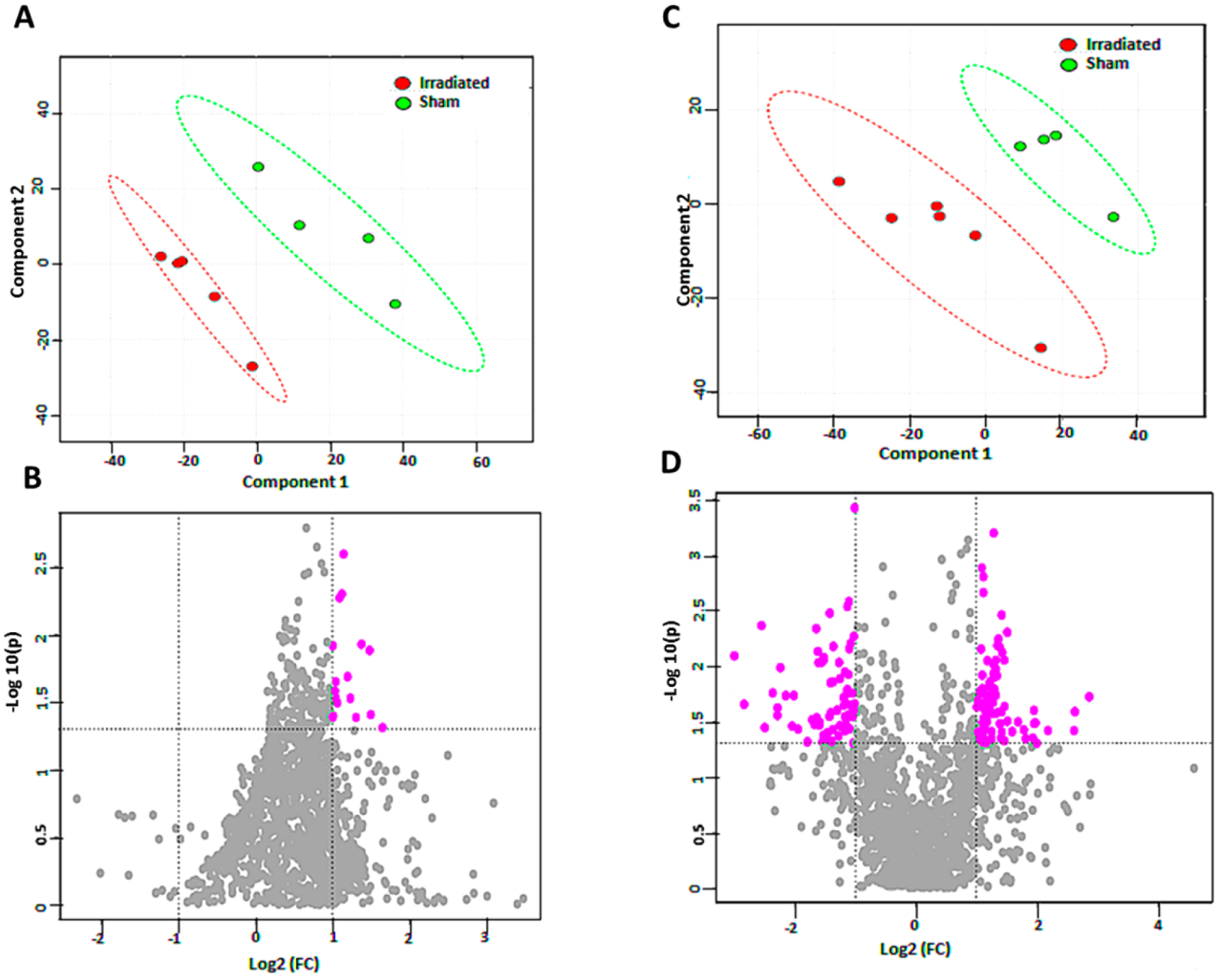

Figure 2. Liver metabolomics of Gfrp knock-in mice shows distinct metabolite profiles in response to radiation exposure. (A,C) PLS-DA score plots comparing metabolite profiles of sham-treated mice with those that were euthanized 24 h and 4 days post radiation exposure, respectively. The R^2 and Q^2 values were 0.95 and 0.75 (A) and 0.96 and 0.45 (B), respectively. (B,D) Volcano plot of liver cell extracts comparing irradiated and sham groups of mice in the same order. The pink dots represent selected putative markers with a *p*-value <0.05 and fold-change cutoff of > or < 2.

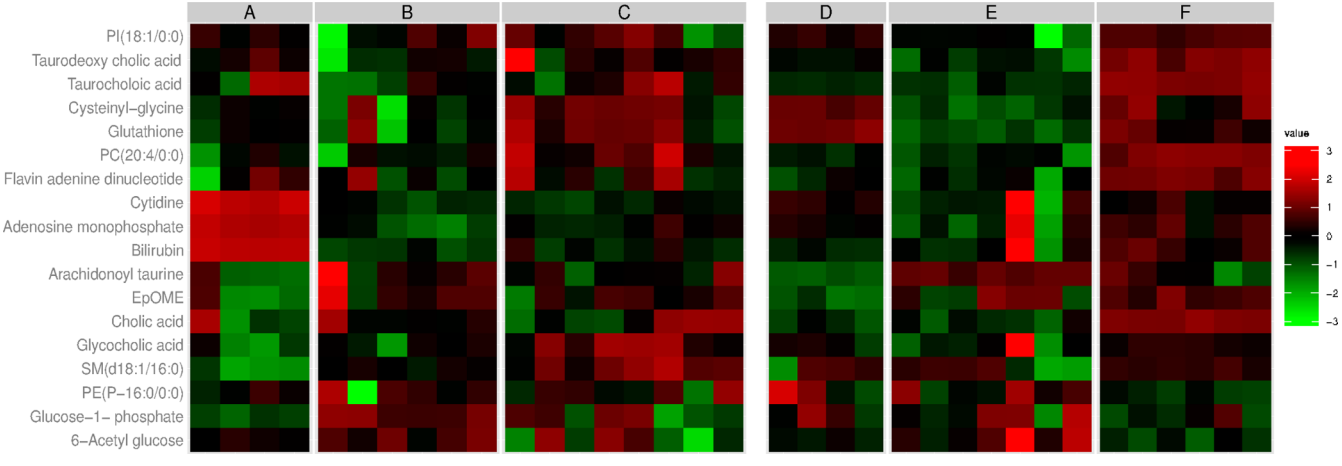

Figure 3. Heat map showing differential abundance of metabolites in response to different time intervals after radiation exposure in Gfrp control and transgenic mice. (A–C) Metabolic profiles of liver tissue from Gfrp−/Cre+ (control) mice that were sham irradiated 24 h and 4 days post radiation exposure, respectively. (D–F) Liver metabolite profiles of Gfrp transgenic mice in the same order. Each column represents a sample, and each row represents a metabolite. The mean signal intensity is colored black; red indicates above-mean intensity, green denotes below-mean intensity, and the degree of color saturation reflects the magnitude of intensity relative to the mean. Both *p*-values and fold changes are listed in Supplementary Tables 2 and 3.

dx.doi.org/10.1021/pr500278t | *J. Proteome Res.* 2014, 13, 3065–3074

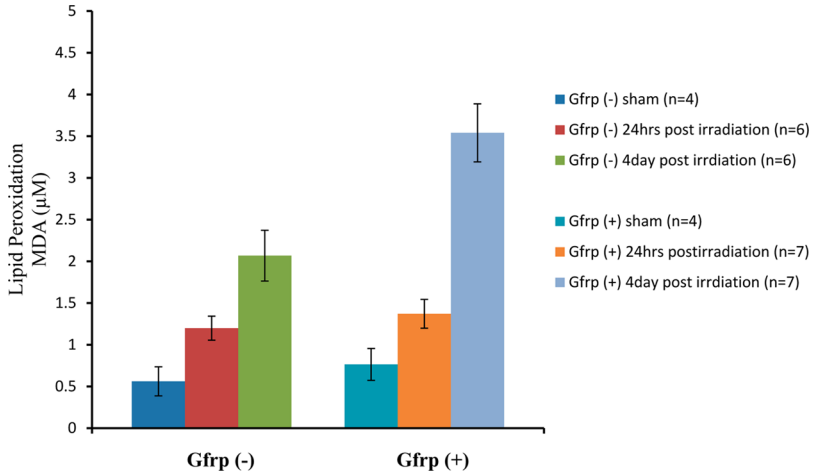

Figure 4. Increased lipid peroxidation seen after radiation exposure. Decomposition of unstable peroxides derived from polyunsaturated fatty acids in the liver tissue homogenates obtained from sham or irradiated mice was measured as malonaldehyde (MDA) equivalents, which is a carbonyl product of lipid peroxides. The lipid peroxidation was found to increase with time after radiation exposure and was genotype dependent. The bars represent the mean ± SD of MDA in each group.

time point in wild-type animals. On the other hand, at 24 h following IR, total GSH levels were significantly decreased (more than 60%) in Gfrp knock-in mouse livers, resulting in a 1.8 fold increase in % GSSG compared to sham-irradiated Gfrp transgenic mice. Although the Gfrp transgenic mice recovered the majority (up to 84%) of their total glutathione pool, the relative GSSG levels were still significantly higher (1.35 fold) than that of sham, 4 days after IR exposure. The dipeptide cysteinyl glycine levels were also markedly decreased within 24 h of radiation exposure in Gfrp transgenic mice. We also determined the change in liver Gfrp expression after 24 h (day 1) and on day 4 after 8.5 Gy of TBI using qRT-PCR in control mice. We observed a significant ($p < 0.0001$) increase in Gfrp expression in liver samples of irradiated control Gfrp mice ($n = 6$) at 24 h compared to unirradiated mice ($n = 3$). However, Gfrp expression reached basal levels in irradiated control Gfrp mice ($n = 6$) by day 4 ($p = 0.074$) (Supplementary Figure 17). On the basis of these results, it may be reasonable to assume that radiation causes an increase in Gfrp expression, which is expected to suppress BH4 bioavailability, resulting in higher oxidative stress in control Gfrp mice. On the other hand, the transgenic Gfrp mice can be expected to have higher susceptibility to IR because of lower basal BH4 levels, which may contribute to IR-induced oxidative damage compared to irradiated control Gfrp littermates. Collectively, our data strongly suggest that Gfrp overexpression exacerbates IR-induced liver tissue injury.

Increased Lipid Peroxidation and Dysregulated Lipid Metabolism in Gfrp Transgenic Mice

Based on the results of untargeted metabolic profiling showing dysregulated lipid metabolism, we interrogated lipid peroxidation as a consequence of radiation-mediated liver injury. Statistical analysis using ANOVA revealed significant accumulation of malondialdehyde in liver homogenates of control and transgenic mice as a function of time after radiation exposure (Figure 4). In addition, we performed stable-isotope-labeled multiple reaction monitoring mass spectrometry to quantitatively assess the differential abundance of lipids, amino acids, biogenic amines, and hexose sugars in these mice before and after radiation. There was a striking down regulation of Lyso PCs and carnitines of varying carbon chain lengths in irradiated Gfrp knock-in mice within 24 h (Supplementary Figure S18 and Supplementary Table T4) and after 4 days of radiation exposure (Figure 5 and Supplementary Table 5) as compared

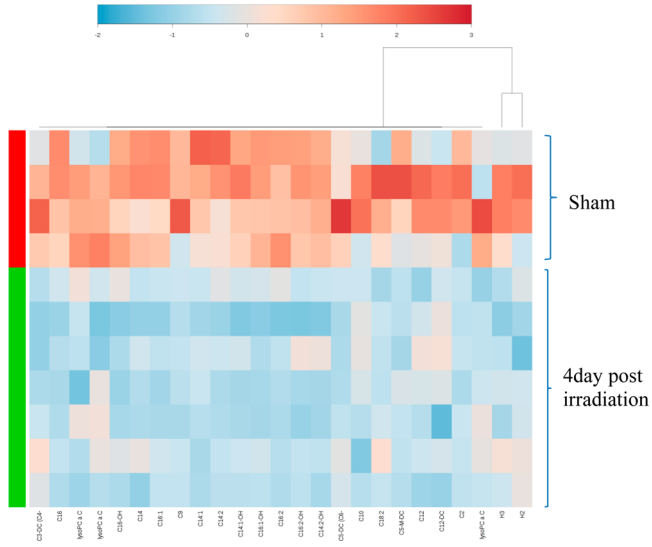

Figure 5. Targeted metabolomics shows down regulation of lipids in irradiated Gfrp transgenic mice. A panel of 25 metabolites showing statistically significant difference in abundance between the sham and irradiated groups of Gfrp transgenic mice are displayed. The metabolites were hierarchically clustered by Ward algorithm using the Euclidian distance. The metabolites are listed in Supplementary Table 4.

to the control littermates, suggesting transgenic Gfrp mice may not be able to protect IR-induced tissue damage as efficiently as the control littermates. In order to address the observed intragroup variability, we included more biological replicates in the treated group, because we expected heterogeneity of the radiation response. Interindividual variability has been well documented in previously published metabolomic studies using mouse models.[25,41]

dx.doi.org/10.1021/pr500278t | J. Proteome Res. 2014, 13, 3065−3074

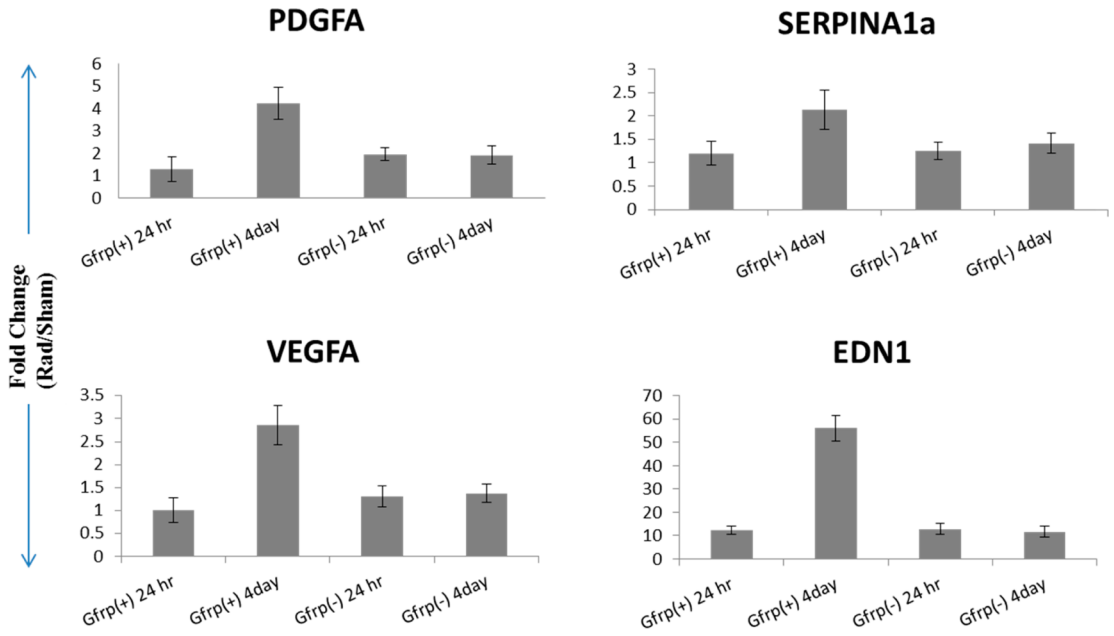

Figure 6. Increased expression of genes associated with liver fibrosis post radiation exposure. RT-PCR-based gene expression profiling was performed with tissue extracts obtained from Gfrp control and knock-in mice with and without radiation exposure (see Materials and Methods) to assess the expression of genes involved in cellular processes that facilitate liver fibrosis.

Radiation Exposure Enhanced Liver Fibrogenic Profile in Gfrp Mice

Since ROS are known to induce modifications in cell structure and function, we next asked whether radiation exposure causes potential changes in liver fibrosis markers. Radiation induced histopathological changes in the liver tissue are not apparent within the first few weeks of radiation exposure, hence we performed RT-PCR-based gene expression profiling for genes involved in facilitating tissue fibrosis, at 24 h and 4 day time points following IR exposure. Our results show that radiation induces the expression of molecular markers of liver fibrosis at day 4 in both control and transgenic mice. However, the expression of vascular endothelial growth factor (VEGF), platelet-derived growth factor (PDGF), serine peptidase inhibitor (SerpinA1a), and endothelin 1 (EDN 1) was significantly higher in Gfrp knock-in mice compared to the wild-type littermates at day 4 (Figure 6). Lipid peroxidation has been shown to increase VEGF expression.[42] Therefore, IR-induced lipid peroxidation in Gfrp transgenic mice may up-regulate the expression of genes involved in liver fibrosis development, thus resulting in an enhanced fibrogenic profile in Gfrp mice.

DISCUSSION

We recently generated a Gfrp-overexpressing transgenic mouse model, which shows decreased levels of tissue BH4 and blood GSH at basal level, suggesting higher oxidative stress.[18] This could be attributed to Gfrp-overexpression-mediated suppression of GTPCH1 enzymatic activity leading to a decrease in cellular BH4 levels, resulting in eNOS uncoupling. Uncoupled eNOS generates more superoxide instead of nitric oxide, causing higher oxidative stress.[43] Furthermore, ionizing radiation is known to induce oxidative stress by impairing the cellular antioxidant machinery and generating more ROS. BH4 is an endogenous natural antioxidant, and studies have shown that radiation causes a decrease in BH4 bioavailability,[17] which may result in higher oxidative stress. In this study, we characterized metabolic changes in the liver following irradiation in control and Gfrp transgenic knock-in mice. The goal was to understand how radiation-mediated liver injury is manifested at the small molecule metabolite level, while also discerning the redox-status-dependent differences in the acute (24 h) and delayed (4 days) radiation response and finally how this response is dictated by the genotype.

The liver is a critical organ for maintaining both metabolic and redox homeostasis. As a result, liver injury due to external insults like radiation exposure can severely compromise carbohydrate, lipid, and single carbon metabolism, ultimately leading to a myriad of pathophysiological conditions, including imbalance in blood glucose levels as well as cellular and brain toxicity. Liver has been reported to be a late responding tissue to radiation stress, and hence we could expect subtle changes, some of which are reversible while other manifest at later time points.[44] There is, however, a lack of understanding of specific metabolic changes in liver tissue after exposure to IR. In addition, to the best of our knowledge, there are no published studies on radiation-induced tissue injury or metabolomics markers of liver damage using an in vivo model system of elevated oxidative stress.

Comparative untargeted metabolomic profiling of the wild type mice showed significant delayed effects after 4 days of radiation exposure but not at 24 h. In contrast, the transgenic mice showed decreased levels of reduced glutathione and increased glycocholic acid and *N*-arachidonoyl taurine within 24 h of radiation exposure, indicating early onset of metabolic dysfunstion. After 4 days, the transgenic mice exhibited elevated levels of FAD (indicating depletion of reduced equivalents), accumulation of bile acids, and a decrease in tissue levels of bilirubin, suggesting progressive liver damage. It is likely that bile accumulation following radiation, which was more significant in Gfrp transgenic mice, accentuates IR-induced oxidative damage and liver tissue injury due to suppressed BH4 bioavailability.

dx.doi.org/10.1021/pr500278t | *J. Proteome Res.* 2014, 13, 3065−3074

We did not find BH4 as a putative biomarker in the untargeted metabolomic profiling experiments; this is expected because BH4 is a redox-sensitive metabolite and needs special experimental conditions to be detected and quantified by mass spectrometry.[45] Furthermore, RT-PCR-based gene expression profiling showed that radiation-induced liver fibrogenic potential was evident for both genotypes 4 days after radiation exposure; however, it was much more pronounced in the transgenic mice. The liver tissue is primarily constituted of differentiated cells; as such, radiation-induced changes of the liver tissue are not apparent within the first few weeks.[19] In addition, liver fibrosis is a delayed effect of radiation; thus hepatic architectural changes that are amenable to detection by histopathology appear 6 to 10 weeks after total body irradiation in mice.[19,46] Mass-spectrometry-based quantitative lipidomics showed a significant down regulation of Lyso PCs and carnitines after radiation exposure, concomitant with a significant increase in lipid peroxidation levels in the transgenic mice following radiation exposure. Thus, these results lend credence to our hypothesis that the transgenic mice are more susceptible to radiation stress. This susceptibility may result in an increase in tissue injury and compromise their ability to mount an appropriate response to combat radiation induced cellular and tissue damage. In addition, our findings underscore the utility of using a multimodal classifier (gene expression plus metabolomics) to assess the early risk of radiation induced tissue injury (which would otherwise be undetectable by histopathology), thus augmenting early therapeutic interventions.

Taken together, these data clearly indicate higher levels of metabolic markers of liver damage in Gfrp knock-in mice as compared to their control littermates as a result of radiation exposure. The decrease in bioavailability of BH4 and its biological implications causing liver damage remain under investigation.

■ ASSOCIATED CONTENT

Supporting Information

List of putative markers of radiation induced liver injury in control and Gfrp transgenic mice (Supplementary Tables 1−3). Fragmentation spectra for metabolites plotted as a heat map in Figure 3 (Supplementary Figures 1−16). qRTPCR analysis of liver Gfrp expression in irradiated and unirradiated control Gfrp mice (Supplementary Figure 17). Heat map showing differentially abundant metabolites in the transgenic mice after 24 h of radiation exposure (Supplementary Figure 18). Targeted metabolomics derived list of differentially abundant metabolites in Gfrp transgenic mice after 24 h and 4 days of radiation exposure (Supplementary Tables 4 and 5). This material is available free of charge via the Internet at http://pubs.acs.org.

■ AUTHOR INFORMATION

Corresponding Author

*E-mail: akc27@georgetown.edu. Fax: (202) 687-8860. Tel.: (202) 687-2756.

Author Contributions

●These authors contributed equally.

Notes

The authors declare no competing financial interest.

■ ACKNOWLEDGMENTS

The authors would like to acknowledge the Proteomics and Metabolomics shared resource partially supported by NIH/NCI grant P30-CA051008 and support to M.H.-J. from NIH/NIAID grant AI67798 and the Veterans Administration.

■ REFERENCES

(1) Kmiec, Z. Cooperation of liver cells in health and disease. *Adv. Anat. Embryol. Cell Biol.* **2001**, *161* (III−XIII), 1−151.
(2) Dawson, L. A.; Ten Haken, R. K.; Lawrence, T. S. Partial irradiation of the liver. *Semin. Radiat. Oncol.* **2001**, *11*, 240−246.
(3) Lin, R. X.; Zhao, H. B.; Li, C. R.; Sun, Y. N.; Qian, X. H.; Wang, S. Q. Proteomic analysis of ionizing radiation-induced proteins at the subcellular level. *J. Proteome Res.* **2009**, *8*, 390−399.
(4) Dawson, L. A.; Normolle, D.; Balter, J. M.; McGinn, C. J.; Lawrence, T. S.; Ten Haken, R. K. Analysis of radiation-induced liver disease using the Lyman NTCP model. *Int. J. Radiat. Oncol. Biol. Phys.* **2002**, *53*, 810−821.
(5) Cheng, J. C.; Wu, J. K.; Huang, C. M.; et al. Radiation-induced liver disease after three-dimensional conformal radiotherapy for patients with hepatocellular carcinoma: dosimetric analysis and implication. *Int. J. Radiat. Oncol. Biol. Phys.* **2002**, *54*, 156−162.
(6) Khan, A. R.; Rana, P.; Devi, M. M. Nuclear magnetic resonance spectroscopy-based metabonomic investigation of biochemical effects in serum of gamma-irradiated mice. *Int. J. Radiat. Biol.* **2011**, *87*, 91−97.
(7) Lanz, C.; Patterson, A. D.; Slavik, J.; et al. Radiation metabolomics. 3. Biomarker discovery in the urine of gamma-irradiated rats using a simplified metabolomics protocol of gas chromatography-mass spectrometry combined with random forests machine learning algorithm. *Radiat. Res.* **2009**, *172*, 198−212.
(8) Liu, H.; Wang, Z.; Zhang, X. Selection of candidate radiation biomarkers in the serum of rats exposed to gamma-rays by GC/TOFMS-based metabolomics. *Radiat. Prot. Dosimetry* **2013**, *154*, 9−17.
(9) Varghese, R. S.; Cheema, A.; Cheema, P. Analysis of LC-MS data for characterizing the metabolic changes in response to radiation. *J. Proteome Res.* **2010**, *9*, 2786−2793.
(10) Patterson, A. D.; Li, H.; Eichler, G. S.; et al. UPLC-ESI-TOFMS-based metabolomics and gene expression dynamics inspector self-organizing metabolomic maps as tools for understanding the cellular response to ionizing radiation. *Anal. Chem.* **2008**, *80*, 665−674.
(11) Coy, S. L.; Cheema, A. K.; Tyburski, J. B.; Laiakis, E. C.; Collins, S. P.; Fornace, A. Radiation metabolomics and its potential in biodosimetry. *Int. J. Radiat. Biol.* **2011**, *87*, 802−823.
(12) Patterson, A. D.; Lanz, C.; Gonzalez, F. J.; Idle, J. R. The role of mass spectrometry-based metabolomics in medical countermeasures against radiation. *Mass Spectrom. Rev.* **2010**, *29*, 503−521.
(13) Thony, B.; Auerbach, G.; Blau, N. Tetrahydrobiopterin biosynthesis, regeneration and functions. *Biochem. J.* **2000**, *347* (Pt 1), 1−16.
(14) Yoneyama, T.; Wilson, L. M.; Hatakeyama, K. GTP cyclohydrolase I feedback regulatory protein-dependent and -independent inhibitors of GTP cyclohydrolase I. *Arch. Biochem. Biophys.* **2001**, *388*, 67−73.
(15) Pathak, R.; Pawar, S. A.; Fu, Q. Characterization of transgenic Gfrp knock-in mice: implications for tetrahydrobiopterin in modulation of normal tissue radiation responses. *Antioxid. Redox Signaling* **2014**, *20*, 1436−1446.
(16) Cohen, S. R.; Cohen, E. P. Chronic oxidative stress after irradiation: an unproven hypothesis. *Med. Hypotheses* **2013**, *80*, 172−175.
(17) Berbee, M.; Fu, Q.; Boerma, M. Reduction of radiation-induced vascular nitrosative stress by the vitamin E analog gamma-tocotrienol: evidence of a role for tetrahydrobiopterin. *Int. J. Radiat. Oncol. Biol. Phys.* **2011**, *79*, 884−891.
(18) Pathak, R.; Pawar, S. A.; Fu, Q.; et al. Characterization of transgenic Gfrp knock-in mice: implications for tetrahydrobiopterin in

modulation of normal tissue radiation responses. *Antioxid. Redox Signaling* **2014**, *20*, 1436−1446.
(19) Wang, S.; Lee, Y.; Kim, J.; et al. Potential role of Hedgehog pathway in liver response to radiation. *PLoS One* **2013**, *8*, e74141.
(20) Kaur, P.; Sheikh, K.; Kirilyuk, A. Metabolomic profiling for biomarker discovery in pancreatic cancer. *Int. J. Mass Spectrom.* **2012**, *310*, 44−51.
(21) Want, E. J.; Wilson, I. D.; Gika, H.; et al. Global metabolic profiling procedures for urine using UPLC-MS. *Nat. Protoc.* **2010**, *5*, 1005−1018.
(22) Smith, C. A.; Want, E. J.; O'Maille, G.; Abagyan, R.; Siuzdak, G. XCMS: processing mass spectrometry data for metabolite profiling using nonlinear peak alignment, matching, and identification. *Anal. Chem.* **2006**, *78*, 779−787.
(23) Ciappio, E. D.; Krausz, K. W.; Rochman, M.; et al. Metabolomics reveals a role for the chromatin-binding protein HMGN5 in glutathione metabolism. *PLoS One* **2014**, *9*, e84583.
(24) Cheema, A. K.; Suman, S.; Kaur, P.; Singh, R.; Fornace, A. J., Jr.; Datta, K. Long-term differential changes in mouse intestinal metabolomics after gamma and heavy ion radiation exposure. *PLoS One* **2014**, *9*, e87079.
(25) Tyburski, J. B.; Patterson, A. D.; Krausz, K. W.; et al. Radiation metabolomics. 2. Dose- and time-dependent urinary excretion of deaminated purines and pyrimidines after sublethal gamma-radiation exposure in mice. *Radiat. Res.* **2009**, *172*, 42−57.
(26) Xia, J.; Mandal, R.; Sinelnikov, I. V.; Broadhurst, D.; Wishart, D. S. MetaboAnalyst 2.0–a comprehensive server for metabolomic data analysis. *Nucleic Acids Res.* **2012**, *40*, W127−W133.
(27) Zhou, B.; Wang, J.; Ressom, H. W. MetaboSearch: tool for mass-based metabolite identification using multiple databases. *PLoS One* **2012**, *7*, e40096.
(28) Illig, T.; Gieger, C.; Zhai, G.; et al. A genome-wide perspective of genetic variation in human metabolism. *Nat. Genet.* **2010**, *42*, 137−141.
(29) Römisch-Margl, W PC; Bogumil, R.; Röhring, C.; Suhre, K. Procedure for tissue sample preparation and metabolite extraction for high-throughput targeted metabolomics. *Metabolomics* **2011**, 1−10.
(30) Xia, J.; Wishart, D. S. Metabolomic data processing, analysis, and interpretation using MetaboAnalyst. . *Curr. Protoc. Bioinformatics* **2011**, No. 10.1002/0471250953.bi1410s34.
(31) Bulmer, A. C.; Verkade, H. J.; Wagner, K. H. Bilirubin and beyond: a review of lipid status in Gilbert's syndrome and its relevance to cardiovascular disease protection. *Prog. Lipid Res.* **2013**, *52*, 193−205.
(32) Condezo-Hoyos, L.; Abderrahim, F.; Conde, M. V.; et al. Antioxidant activity of liver growth factor, a bilirubin covalently bound to albumin. *Free Radical Biol. Med.* **2009**, *46*, 656−662.
(33) MacLean, P. D.; Drake, E. C.; Ross, L.; Barclay, C. Bilirubin as an antioxidant in micelles and lipid bilayers: its contribution to the total antioxidant capacity of human blood plasma. *Free Radical Biol. Med.* **2007**, *43*, 600−609.
(34) Muchova, L.; Vanova, K.; Zelenka, J. Bile acids decrease intracellular bilirubin levels in the cholestatic liver: implications for bile acid-mediated oxidative stress. *J. Cell Mol. Med.* **2011**, *15*, 1156−1165.
(35) Postic, C.; Dentin, R.; Girard, J. Role of the liver in the control of carbohydrate and lipid homeostasis. *Diabetes Metab.* **2004**, *30*, 398−408.
(36) Ljubuncic, P.; Said, O.; Ehrlich, Y.; Meddings, J. B.; Shaffer, E. A.; Bomzon, A. On the in vitro vasoactivity of bile acids. *Br. J. Pharmacol.* **2000**, *131*, 387−398.
(37) Le Quere, V.; Plee-Gautier, E.; Potin, P.; Madec, S.; Salaun, J. P. Human CYP4F3s are the main catalysts in the oxidation of fatty acid epoxides. *J. Lipid Res.* **2004**, *45*, 1446−1458.
(38) Calder, P. C. *n*-3 polyunsaturated fatty acids, inflammation, and inflammatory diseases. *Am. J. Clin. Nutr.* **2006**, *83*, 1505S−1519S.
(39) Fuchs, B.; Schiller, J.; Wagner, U.; Hantzschel, H.; Arnold, K. The phosphatidylcholine/lysophosphatidylcholine ratio in human plasma is an indicator of the severity of rheumatoid arthritis: investigations by 31P NMR and MALDI-TOF MS. *Clin. Biochem.* **2005**, *38*, 925−933.
(40) Wymann, M. P.; Schneiter, R. Lipid signalling in disease. *Nat. Rev. Mol. Cell Biol.* **2008**, *9*, 162−176.
(41) Tyburski, J. B.; Patterson, A. D.; Krausz, K. W.; et al. Radiation metabolomics. 1. Identification of minimally invasive urine biomarkers for gamma-radiation exposure in mice. *Radiat. Res.* **2008**, *170*, 1−14.
(42) Negre-Salvayre, A.; Auge, N.; Ayala, V.; et al. Pathological aspects of lipid peroxidation. *Free Radical Res.* **2010**, *44*, 1125−1171.
(43) Topal, G.; Brunet, A.; Millanvoye, E.; et al. Homocysteine induces oxidative stress by uncoupling of NO synthase activity through reduction of tetrahydrobiopterin. *Free Radical Biol. Med.* **2004**, *36*, 1532−1541.
(44) Zhao, W.; Robbins, M. E. Inflammation and chronic oxidative stress in radiation-induced late normal tissue injury: therapeutic implications. *Curr. Med. Chem.* **2009**, *16*, 130−143.
(45) Zhao, Y.; Cao, J.; Chen, Y. S.; et al. Detection of tetrahydrobiopterin by LC-MS/MS in plasma from multiple species. *Bioanalysis* **2009**, *1*, 895−903.
(46) O'Sullivan, B.; Levin, W. Late radiation-related fibrosis: pathogenesis, manifestations, and current management. *Semin. Radiat. Oncol.* **2003**, *13*, 274−289.